October, 2007

Studies of a lattice model of water confined in a slit pore

Peter A Monson, *University of Massachusetts - Amherst*
J. -C. Liu
Frank van Swol

Studies of a Lattice Model of Water Confined in a Slit Pore†

J.-C. Liu‡ and P. A. Monson*

Department of Chemical Engineering, University of Massachusetts, Amherst, Massachusetts 01003

Frank van Swol

Sandia National Laboratories, P.O. Box 5800, Albuquerque, New Mexico 87185 and Chemical and Nuclear Engineering Department, University of New Mexico, Albuquerque, New Mexico 87131

Received: May 17, 2007; In Final Form: July 25, 2007

We describe an extension of the Bell−Salt lattice model of water to the study of water confined in a slit pore. Wall−fluid interactions are chosen to be qualitatively representative of water interacting with a graphite surface. We have calculated the bulk vapor−liquid phase coexistence for the model through direct Monte Carlo simulations of the vapor−liquid interface. Adsorption and desorption isotherms in the slit pore were calculated using grand canonical ensemble Monte Carlo simulations. In addition, the thermodynamic conditions of vapor−liquid equilibrium for the confined fluid were determined. Our results are consistent with recent calculations for off-lattice models of confined water that show metastable vapor states of confined water persisting beyond the bulk saturation conditions, except for the narrowest pores. The results are similarly consistent with recent experiments on water adsorption in graphitized carbon black.

I. Introduction

There has been substantial interest in the use of lattice models for inhomogeneous fluids. This has been motivated by the simplicity of such models and the opportunity that they present to address relatively large systems which can bridge the nanoscopic and mesoscopic length scales. Examples of recent applications include fluids in ordered pore structures,[1−13] fluids in disordered porous materials[14−19] and nanoscale liquid droplets on solid surfaces.[20,21] Most of this work has focused on simple fluids modeled by orientation independent nearest neighbor interactions, but it is also of interest to investigate more complex lattice models such as that which might be applied to inhomogeneous water.

Among the most widely studied lattice models of water are those based on ideas developed by Bell and his co-workers.[22−31] The basic idea in such models is to introduce orientation dependent attractions between nearest neighbor sites on a bcc lattice.[22] By restricting the hydrogen bonding interactions for each site to be with four tetrahedrally coordinated nearest neighbor sites, the low coordination number interactions in fluid and solid water can be modeled. An expanded structure in which only one of the diamond sublattices of the bcc lattice is occupied can be stabilized by introducing a three-body repulsion[22] or a next nearest neighbor repulsion[23,29] that suppresses simultaneous occupancy of both diamond sublattices. Numerical studies of the Bell water models reveal that they exhibit water-like behavior in their thermodynamic properties including a density maximum in the liquid phase and solid melting by compression.[29,31,32]

In this paper, we consider the Bell−Salt lattice model[23] of water under conditions of confinement in a slit pore. By comparing the behavior of the model with that observed for off-lattice models of carbon slit pores,[33−35] we investigate the applicability of the lattice model as a qualitative model of water under confinement. One key issue to be understood here is whether or not water can condense in a material such as carbon with which it does not hydrogen bond. Another is the relevance of equilibrium pore condensation (EPC) versus hysteresis in the interpretation of experimental results. These issues are central in understanding experimental results for water adsorption in ordered carbon materials[36−40] such as carbon nanotubes in comparison with those for activated carbons.[41−44]

In recent work,[35] two of us studied the properties of three off-lattice models of water confined in slit pores, with the solid−fluid potential chosen to model the interaction of water with a graphite surface. For a given temperature, pore condensation was determined both in terms of the end point of the adsorption branch in the hysteresis loop (for convenience we will refer to this as hysteresis pore condensation or HPC) and in terms of the EPC transition, the latter determined by the chemical potential or bulk pressure where low density (vapor-like) and high density (liquid-like) states of the confined fluid can coexist in equilibrium. It was argued that HPC is more relevant to experiments, where EPC is not accessible on adsorption because of the metastability of the low density (vapor-like) states of the confined fluid. For wider pores, it was observed that HPC occurred for states above the bulk vapor pressure but for narrower pores it could occur for states below the bulk vapor pressure. The behavior for narrower pores was interpreted in terms of the influence of the surface field from both pore walls upon a single layer of water molecules.[34,35] The results for wider pores are consistent with experiments on water adsorption in graphitized carbon black,[45] which feature mesopore/macropore condensation occurring at states above the bulk vapor pressure.

In this work, Monte Carlo simulations have been used to study the Bell−Salt lattice model of water in both bulk and confined states. We have used grand canonical ensemble Monte Carlo

† Part of the "Keith E. Gubbins Festschrift".

* Author to whom correspondence should be addressed.

‡ Present Address: Department of Chemical Engineering, University of Pittsburgh, Pittsburgh, Pennsylvania 15260.

10.1021/jp0738309 CCC: $37.00
Published on Web 10/03/2007

(GCMC) simulations to determine density versus chemical potential isotherms. In addition, we have performed canonical ensemble simulations to determine the vapor−liquid density profiles as a means of establishing phase coexistence conditions for bulk and confined fluids. We find that to a significant extent the confined Bell−Salt model exhibits the qualitative behavior seen in off-lattice models, with respect to both adsorption−desorption hysteresis and EPC.

The remainder of this paper is organized as follows. In the next section, we describe the lattice model in more detail and Monte Carlo simulation methodologies used to study it. In section III, we present our results both for the model in the bulk and for its behavior when confined in slit pores. Section IV gives a summary of our results and conclusions.

II. Lattice Model and Monte Carlo Simulations

A. Model. The lattice model for water we used was developed by Bell and Salt[23,29] and is a modification of an earlier model by Bell.[22] The model uses a bcc lattice with three types of interaction, a nearest neighbor attraction with energy $-\epsilon_{ff}$, an orientation dependent nearest neighbor attraction with energy $-\epsilon_{hb}$, and a next nearest neighbor repulsion with energy ϵ_{nnn}. Each molecule has four tetrahedrally coordinated bonding arms. Two of these are labeled "+", and the other two are labeled "−". This leads to twelve possible orientations in which the bonding arms are aligned with the nearest neighbor vectors. Nearest neighbor attractions modeling hydrogen bonds are formed when pairs of occupied nearest neighbor sites are configured with a "+" arm from one site and a "−" arm from the other site aligned with the nearest neighbor vector. The lattice model Hamiltonian can be expressed as

$$H = -\sum_{i<j}{}' n_i n_j [\epsilon_{ff} + \epsilon_{hb} f_{ij}] + \epsilon_{nnn} \sum_{i<j}{}'' n_i n_j \qquad (1)$$

where n_i and n_j denote the occupancies of sites i and j, either 1 or 0, respectively. $f_{ij} = 1$ if a "+" arm from one site and a "−" arm from the other site are aligned with the nearest neighbor vector between sites i and j, and $f_{ij} = 0$ otherwise. The prime on the first summation denotes a restriction to pairs of sites that are nearest neighbors while the double prime on the second summation denotes a restriction to pairs of sites that are next nearest neighbors.

The bcc lattice can be viewed as two interpenetrating diamond sublattices. The second neighbor repulsions in the model suppress the simultaneous occupancy of the two diamond sublattices, giving a region of stability to an ice-I-like phase. The fully occupied lattice with two hydrogen bonds per site corresponds to ice-VII. The solid−fluid interaction with the pore walls is a nearest neighbor attraction with energy $-\epsilon_{sf}$. We discuss the choice of these parameters below.

B. Monte Carlo Simulations. As noted earlier in studying models of pore condensation, it is essential to have knowledge of the bulk phase behavior. Therefore, we have used Monte Carlo simulations to estimate the bulk coexistence conditions for the model. First, we performed grand canonical Monte Carlo (GCMC) simulations for a cubic bulk system of 40^3 lattice constants in periodic boundary conditions to obtain isotherms of the density (fractional occupancy) versus chemical potential, μ, or activity, $\lambda = \exp(\mu/kT)$. These isotherms exhibit hysteresis below the bulk critical temperature as shown in Figure 1. This hysteresis is due to the fact that the large scale density fluctuations associated with the vapor−liquid phase change are rare events in the Metropolis method.[46] It can be eliminated by using more sophisticated sampling techniques, but that is unnecessary here. Second, we performed canonical Monte Carlo (CMC) simulations to study the vapor−liquid interface of the model at several temperatures. Using these simulations, we could extract the coexistence densities at each temperature from the vapor−liquid density profiles. For these CMC simulations, we used a simulation cell of 40 × 40 × 120 lattice constants. The simulations were initialized by filling a block of sites (40 × 40 × 40 or 40 × 40 × 60 lattice constants) in the central part of the system. Using the density versus chemical potential isotherms from the GCMC simulations, we could then determine the chemical potential at bulk vapor−liquid coexistence. In order to check the accuracy of this approach, we carried out the same procedure for the bcc lattice gas with only nearest neighbor attractions and verified that we could reproduce the rather precise results available from series expansions.[47]

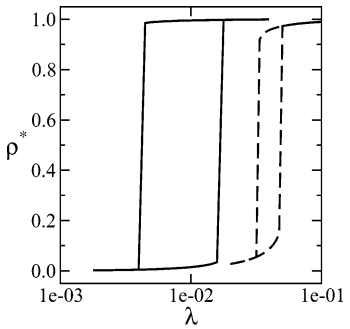

Figure 1. Bulk-phase GCMC simulation results for the reduced density (fractional occupancy), ρ^*, vs activity, $\lambda = \exp(\mu/kT)$, of the lattice model of water. Solid line: $T^* = 1.5$. Dashed line: $T^* = 2.0$.

The calculations of the adsorption/desorption isotherms and vapor−liquid equilibrium in slit pores are similar to that for the bulk phase described above. The wall dimensions were set to be 40 lattice constants in x and y directions with periodic boundary conditions. The system boundaries were aligned with 100 planes of the bcc lattice. For the slit pores, the two layers of sites constituting the pore walls are separated by a pore width, H, which is defined as the number of lattice units in z direction. The pore widths we have studied are 1.5, 2.5, 3.5, 4.5, and 6.5 lattice constants, corresponding approximately to a range of 0.5−2.1 nm in real units (the unit conversion is based upon nearest neighbor distances in liquid water and ice of about 0.28 nm[48]) and comparable to the pore dimensions used in recent studies of off-lattice models.[34,35] These pore widths can accommodate 2, 4, 6, 8, and 12 layers of sites between the walls, respectively. It requires two layers of sites on the bcc lattice to create a single layer of hydrogen-bonded water molecules on a diamond sublattice. For the vapor−liquid interface simulation in the slit pores, the wall dimensions were set to 40 lattice constants in the x direction and 80 or 120 lattice constants in the y direction. The vapor−liquid interface simulations for the slit pore were initialized by filling a block of sites (40 × 40 × 40 or 40 × 40 × 80 lattice constants) in the central part of the system.

The run lengths used in our simulations were typically 2×10^5 steps for the GCMC simulations and 4×10^5 steps for the CMC simulations, with half the steps used for equilibration. Each step consists of M trial configurations, where M is the number of sites on the lattice. For the GCMC simulations, trial configurations were generated either by an attempt to reverse the occupancy of a site in the system or by an attempt to change the orientation at an occupied site in the system. These two types of move were chosen with equal probability. For the CMC simulations, trial configurations were generated either by an attempt to swap the occupancy of an occupied site with that of

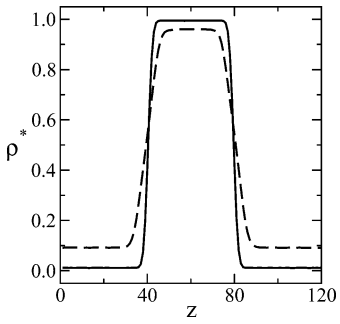

Figure 2. Density, ρ^*, profiles from interface simulations for the lattice model of water. Solid line: $T^* = 1.5$. Dash line: $T^* = 2.0$.

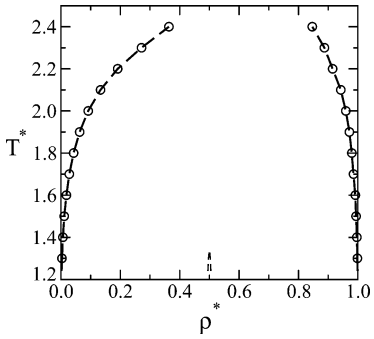

Figure 3. Bulk temperature, T^*, vs density, ρ^*, coexistence diagram for the lattice model of water. At low temperature a region of stability for the ice-I-like phase is seen.

an unoccupied site or by an attempt to change the orientation at an occupied site in the system. In all cases, the type of trial move was chosen randomly with uniform probability.

III. Results and Discussion

A. Bulk Properties. Borick and Debenedetti[31] have studied the phase behavior of the Bell−Salt model using a cluster-variation method, and we have used their work as an initial guide to the behavior of the model. They found four different types of phase behavior, one of which is water-like. We have investigated a series of values of temperature ($T^* = kT/\epsilon_{ff}$), $\epsilon_{nnn}/\epsilon_{ff}$, and $\epsilon_{HB}/\epsilon_{ff}$ and have found a set of parameters ($\epsilon_{hb}/\epsilon_{ff} = 4$ and $\epsilon_{nnn}/\epsilon_{ff} = 0.63$) for which the system has a vapor−liquid critical point and a triple point with the appearance of an ice-I-like ordered phase of density intermediate between that of the fluid phases. In this ice-I-like phase, only one of the diamond sublattices is occupied. As expected for a lattice model, the dense "liquid" phase has significant solid-like character, with substantial orientational ordering and occupancy of both diamond sublattices. Figures 1 and 2 show density (expressed as fractional occupancy, ρ^*, of the bcc lattice) versus activity isotherms and vapor−liquid density profiles for two temperatures using these model parameters. As described above, we can use these results to determine the phase coexistence activity and densities. Figure 3 shows the density versus temperature coexistence phase diagram for the fluid states and also a region of stability for the ice-I-like phase at low temperature and fractional occupancy close to 0.5. Figure 4 shows the saturation activity, λ_0, versus temperature diagram for fluid phase equilibrium in the model.

B. Confined Systems. For the interaction with the walls of the slit pore we have, in the first instance, used $\epsilon_{sf}/\epsilon_{ff} = 1.5$, corresponding roughly to the value expected for water interacting with a graphite surface. Adsorption/desorption isotherms for four values of H are shown in Figure 5 at $T^* = kT/\epsilon_{ff} = 1.5$. The density is plotted versus the relative activity, λ/λ_0, which is equivalent to relative pressure except for the (small) effect of gas imperfection. We see that in all of these cases the isotherms exhibit hysteresis, with the width of the hysteresis increasing with increasing pore width. For the narrower pores, $H = 2.5$ and $H = 3.5$, HPC occurs for relative activities below bulk saturation. For the wider pores, HPC pore condensation occurs for relative activities above bulk saturation.

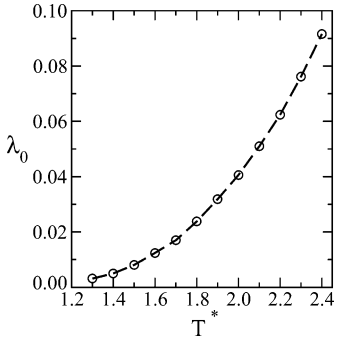

Figure 4. Bulk saturation activity, λ_0, vs temperature, T^*, for the lattice model of water.

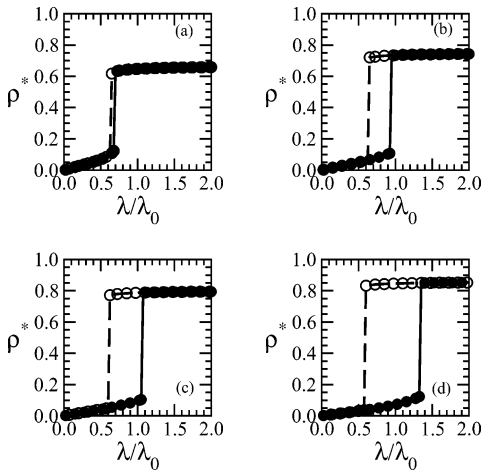

Figure 5. Adsorption/desorption isotherms for lattice model of water confined in slit pores with $\epsilon_{sf}/\epsilon_{ff} = 1.5$. (a) $H = 2.5$; (b) $H = 3.5$; (c) $H = 4.5$; and (d) $H = 6.5$. The density, ρ^*, is plotted versus the relative activity, λ/λ_0. The filled circles are adsorption results, and the open circles are desorption results. Lines are drawn as a guide to the eye.

These results are qualitatively consistent with those we obtained recently for some off-lattice models of water in slit pores.[35] We can interpret these results in two ways. On the one hand, we can view the narrowing of the hysteresis region with decreasing pore width in terms of the approach to the pore critical point under increasing confinement.[49,50] On the other hand, we can think in terms of the solid−fluid interactions facilitating condensation for narrower pores, a mechanism addressed in earlier work on off-lattice models.[34,35] Figure 6 shows isotherms for $H = 2.0$ and $H = 1.5$. In both cases, the hysteresis has disappeared. This behavior, which differs from what is observed for off-lattice models,[34,35] is a consequence of the low probability of configurations where hydrogen bond interactions can occur for this lattice model when there are just a few layers of sites. This feature tends to suppress the vapor−liquid transition for narrow pores.

Vapor−liquid density profiles for the confined systems from CMC simulations are shown in Figure 7 for four pore widths corresponding to those in Figure 5. In these profiles, the density parallel to the pore walls in the y direction is shown averaged in the $x-z$ plane. We note that the width of the interfacial region

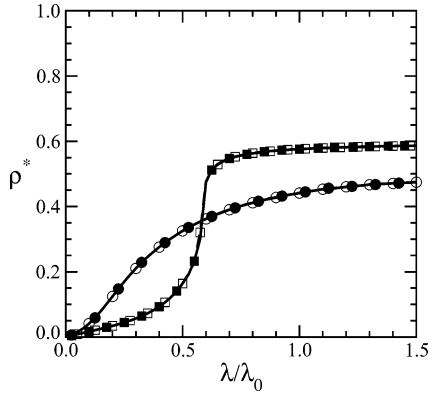

Figure 6. Adsorption/desorption isotherms for the lattice model of water confined in slit pores with $H = 1.5$ (circles) and $H = 2.0$ (squares) with $\epsilon_{sf}/\epsilon_{ff} = 1.5$. The density, ρ^*, is plotted versus the relative activity, λ/λ_0. The filled symbols are adsorption results, and the open symbols are desorption results; no hysteresis is seen in these cases. The lines are drawn as a guide to the eye.

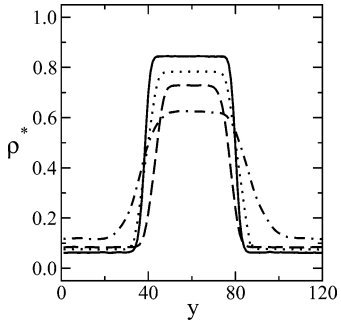

Figure 7. Density, ρ^*, profiles from interface simulations for the lattice model of water confined in slit pores with $\epsilon_{sf}/\epsilon_{ff} = 1.5$. Dotted-dashed line, $H = 2.5$; dashed line, $H = 3.5$; dotted line, $H = 4.5$; and full line, $H = 6.5$.

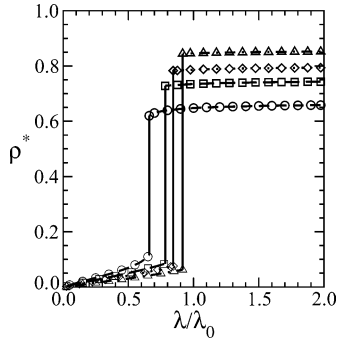

Figure 8. Equilibrium isotherms for the lattice model of water confined in slit pores with $\epsilon_{sf}/\epsilon_{ff} = 1.5$. Circles: $H = 2.5$. Squares: $H = 3.5$. Diamonds: $H = 4.5$. Triangles: $H = 6.5$. The density, ρ^*, is plotted versus the relative activity, λ/λ_0. Lines are drawn as a guide to the eye.

gets progressively larger as the pore gets narrower and we approach a pore critical point. The vapor−liquid interface in the confined system is nonplanar, and this will increase the width of these profiles depending on the curvature of the meniscus. The flat parts of these profiles correspond to the phase coexistence densities for the pore fluid. Using these densities, we can identify the states in Figure 5 corresponding to vapor−liquid equilibrium in the pores (EPC), and we can redraw the isotherms with the metastable states removed as shown in Figure 8. We have a single step in each isotherm corresponding to the equilibrium vapor−liquid phase transition for the confined fluid. In each case, EPC occurs for activities below bulk saturation, with the EPC transition approaching λ_0 with increasing pore size. We return to this observation and its significance below.

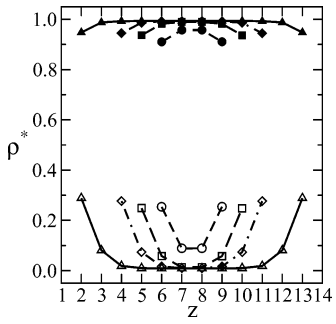

Figure 9. Density, ρ^*, distributions in a direction normal to the pore walls corresponding to liquid and vapor states at equilibrium for the lattice model of water confined in slit pores with $\epsilon_{sf}/\epsilon_{ff} = 1.5$. Filled symbols are for the liquid phase, and open symbols are for the vapor phase. Circles: $H = 2.5$. Squares: $H = 3.5$. Diamonds: $H = 4.5$. Triangles: $H = 6.5$. Lines are drawn as a guide to the eye. For $H = 2.5$, $H = 3.5$, and $H = 4.5$, the symbols and lines are moved to the center of the figure for clarity.

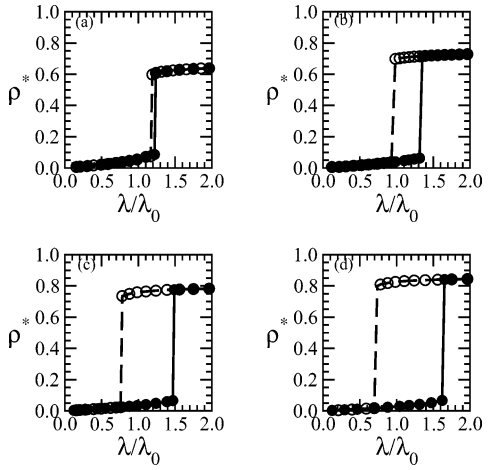

Figure 10. Adsorption/desorption isotherms for the lattice model of water confined in slit pores with $\epsilon_{sf}/\epsilon_{ff} = 1$. (a) $H = 2.5$; (b) $H = 3.5$; (c) $H = 4.5$; and (d) $H = 6.5$. The density, ρ^*, is plotted versus the relative activity, λ/λ_0. The filled circles are adsorption results, and the open circles are desorption results. Lines are drawn as a guide to the eye.

We have also calculated density profiles in a direction normal to the pore walls, and averaged over the $x-y$ plane, for the phase equilibrium states given in Figure 8. Figure 9 shows the density profiles for the saturated liquid and vapor states for the different values of H. For the liquid state, the density in the layer near the wall is lower than that away from the wall, because of the loss of "hydrogen bonds" in that layer. For the vapor state, the density is much higher near the wall, reflecting greater importance of the solid−fluid interactions relative to the hydrogen bonding at low density.

Adsorption/desorption isotherms for a weaker surface field, $\epsilon_{sf}/\epsilon_{ff} = 1$, are shown in Figure 10. In this case, the HPC occurs for activities greater than bulk saturation. The results are otherwise similar to those in Figure 5. The equilibrium isotherms are shown in Figure 11. We see that EPC occurs above bulk saturation for all cases, a situation that is sometimes called capillary evaporation.[51] This latter terminology arises from thinking about the system from the perspective of approaching bulk saturation from a compressed liquid state. The differences in the results for the two surface fields reflect the fact that a weaker surface field moves the stability range of dense fluid states to higher relative activity for a given temperature.

Our previous work on water in slit pores was motivated by the question of whether water should condense below bulk

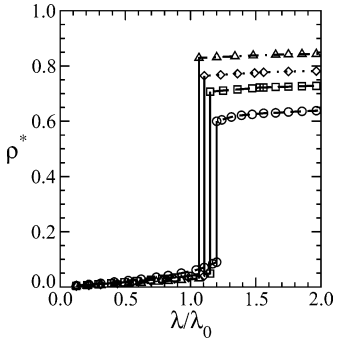

Figure 11. Equilibrium isotherms for the lattice model of water confined in slit pores with $\epsilon_{sf}/\epsilon_{ff} = 1$. The density, ρ^*, is plotted versus the relative activity, λ/λ_0. Circles: $H = 2.5$. Squares: $H = 3.5$. Diamonds: $H = 4.5$. Triangles: $H = 6.5$. Lines are drawn as a guide to the eye.

saturation for carbon adsorbents. As mentioned earlier, experimental results for water in graphitized carbon black show hysteresis in which pore condensation occurs above saturation.[45] Both in our earlier work and in the present model, for $\epsilon_{sf}/\epsilon_{ff} = 1.5$, the results from HPC and EPC lead to conflicting conclusions. The HPC results indicate pore condensation above λ_0 for wider pores and pore condensation below λ_0 for narrower pores. In both models, the EPC occurs below λ_0. Which of these results is more relevant to experiment? As we stated in our earlier paper,[35] we believe the hysteresis loops are the best guide. When we study vapor−liquid equilibrium for bulk fluids, it is always possible to place the phases in contact, allowing the direct location of the phase coexistence. For fluids in porous materials where pore condensation occurs, isotherms are routinely accompanied by hysteresis, and it is generally not possible to achieve equilibrium vapor−liquid coexistence during adsorption (for systems where the pore fluid has unrestricted contact with the bulk phase, e.g., fluids confined in open-ended cylindrical pores such as in MCM-41, desorption is expected to occur at the EPC transition[52]). Thus, as a practical matter, whether or not water condenses in carbon pores below bulk saturation is determined by the location of the end point of the adsorption branch in the hysteresis loop.

Equilibrium condensation for water in a carbon slit pore for activities below λ_0 should not necessarily be viewed as a surprising result given that the contact angle, θ, for water on a free surface of graphite is about 86°.[53] The Kelvin equation, which is presumably valid for wide pores, predicts that the relative activity for pore condensation in a slit pore is given by

$$kT \ln\left(\frac{\lambda}{\lambda_0}\right) = \frac{-2\sigma_{VL} \cos\theta}{\rho_L r} \qquad (2)$$

where σ_{VL} is the vapor−liquid surface tension, ρ_L is the density of the bulk liquid, and r is the pore radius. Contact angles less than 90° lead to EPC for $\lambda < \lambda_0$ while contact angles greater than 90° lead to EPC for $\lambda > \lambda_0$. This prediction is independent of whether or not (as in this case) the equation is corrected for the thickness of the adsorbed layer on the pore surface. Departures from the Kelvin equation for narrow pores are well-documented,[49,50] but the qualitative prediction about the link between the free surface contact angle and the location of the EPC transition with respect to bulk saturation should still hold.

IV. Summary and Conclusions

We have made a study of the Bell−Salt lattice model of water extended to the case of confinement in a slit pore, focusing on the nature of the pore condensation transition. GCMC simulations of the adsorption/desorption isotherms exhibit hysteresis, with the width of the hysteresis decreasing with decreasing pore size. For narrow pores, the vapor branch of the hysteresis loop terminates at relative activities below those corresponding to bulk saturation conditions, while for wider pores, this happens for supersaturated bulk states, in agreement with earlier simulations of off-lattice models[35] and experiments on water adsorption on graphitized carbon black.[45]

We have also determined the conditions of vapor−liquid equilibrium for both the bulk and the confined fluids. We have found that the EPC occurs before bulk saturation for the systems studied with the stronger surface field. For water in graphite-like pores, such behavior would be expected on the basis of values of the contact angle and consideration of the Kelvin equation. For a weaker surface field, we have found that pore condensation, whether EPC or HPC, occurs for supersaturated bulk states. This is a result of the weaker surface field requiring higher chemical potentials for stability of dense fluid states in the pores.

In general, the Bell−Salt model under confinement in a slit pore yields similar qualitative behavior to off-lattice models. However, the model seems to be less realistic for the narrowest pores. At the temperature we have considered, the Bell−Salt model requires at least four layers of sites on the bcc lattice ($H = 2.5$), allowing the formation of two layers of hydrogen-bonded water molecules, for a vapor−liquid transition to occur. This is due to the configurational limitations of the lattice and restrictions on the ways in which hydrogen bonds can be formed. Whether this is intrinsic to the lattice approach or merely a feature of this particular model will be a worthwhile topic for additional research.

Acknowledgment. This work was supported at the University of Massachusetts by the U.S. Army Research Office (Grant DAAD19-02-1-0384) and the National Science Foundation (Grant CBET-0649552) and at Sandia by the DOE office of Basic Energy Sciences, Division of Material Sciences and Engineering, the DOE Office of Science Advanced Scientific Computing Research (ASCR) program in Applied Mathematical Sciences. Sandia is a multiprogram laboratory operated by Sandia Corporation, a Lockheed-Martin Company, for the U.S. DOE under Contract No. DE-AC04-94AL85000.

References and Notes

(1) Marconi, U. M. B.; van Swol, F. *Europhys. Lett.* **1989**, *8* (6), 531−535.
(2) Marconi, U. M. B.; van Swol, F. *Phys. Rev. A* **1989**, *39* (8), 4109−4116.
(3) Bock, H.; Schoen, M. *J. Phys.: Condens. Matter* **2000**, *12* (8), 1569−1594.
(4) Rocken, P.; Tarazona, P. *J. Chem. Phys.* **1996**, *105* (5), 2034−2043.
(5) Schoen, M.; Bock, H. *J. Phys.: Condens. Matter* **2000**, *12* (8A), A333−A338.
(6) Aranovich, G.; Donohue, M. *J. Colloid Interface Sci.* **1998**, *200* (2), 273−290.
(7) Aranovich, G. L.; Donohue, M. D. *Phys. Rev. E* **1999**, *60* (5), 5552−5560.
(8) Aranovich, G. L.; Donohue, M. D. *J. Colloid Interface Sci.* **1997**, *189* (1), 101−108.
(9) Leung, K.; Luzar, A. *J. Chem. Phys.* **2000**, *113* (14), 5845−5852.
(10) Luzar, A.; Leung, K. *J. Chem. Phys.* **2000**, *113* (14), 5836−5844.
(11) Malanoski, A. P.; van Swol, F. *Phys. Rev. E* **2002**, *66* (4), 041602.
(12) Malanoski, A. P.; van Swol, F. *Phys. Rev. E* **2002**, *66* (4), 041603.
(13) Libby, B.; Monson, P. A. *Langmuir* **2004**, *20* (10), 4289−4294.
(14) Woo, H. J.; Sarkisov, L.; Monson, P. A. *Langmuir* **2001**, *17* (24), 7472−7475.
(15) Kierlik, E.; Monson, P. A.; Rosinberg, M. L.; Sarkisov, L.; Tarjus, G. *Phys. Rev. Lett.* **2001**, *8705* (5), 055701.

(16) Kierlik, E.; Monson, P. A.; Rosinberg, M. L.; Tarjus, G. *J. Phys.: Condens. Matter* **2002**, *14* (40), 9295−9315.
(17) Sarkisov, L.; Monson, P. A. *Phys. Rev. E* **2002**, *65* (1), 011202.
(18) Woo, H. J.; Monson, P. A. *Phys. Rev. E* **2003**, *67* (4), 041207.
(19) Porcheron, F.; Monson, P. A.; Thommes, M. *Langmuir* **2004**, *20* (15), 6482−6489.
(20) Porcheron, F.; Monson, P. A. *Langmuir* **2006**, *22* (4), 1595−1601.
(21) Porcheron, F.; Monson, P. A.; Schoen, M. *Phys. Rev. E* **2006**, *73* (4), 041603.
(22) Bell, G. M. *J. Phys. C: Solid State Phys.* **1972**, *5* (9), 889−905.
(23) Bell, G. M.; Salt, D. W. *J. Chem. Soc.: Faraday Trans. 2* **1976**, *72*, 76−86.
(24) Lavis, D. A.; Christou, N. I. *J. Phys. A: Math. Gen.* **1979**, *12* (10), 1869−1890.
(25) Lavis, D. A.; Christou, N. I. *J. Phys. A: Math. Gen.* **1977**, *10* (12), 2153−2169.
(26) Lavis, D. A.; Southern, B. W. *J. Stat. Phys.* **1984**, *35* (5−6), 489−506.
(27) Lavis, D. A. *J. Phys. C: Solid State Phys.* **1973**, *6* (9), 1530−1545.
(28) Meijer, P. H. E.; Kikuchi, R.; Vanroyen, E. *Phys. A* **1982**, *115* (1−2), 124−142.
(29) Meijer, P. H. E.; Kikuchi, R.; Papon, P. *Phys. A* **1981**, *109* (3), 365−381.
(30) Borick, S. S.; Debenedetti, P. G.; Sastry, S. *J. Phys. Chem.* **1995**, *99* (11), 3781−3792.
(31) Borick, S. S.; Debenedetti, P. G. *J. Phys. Chem.* **1993**, *97* (23), 6292−6303.
(32) Bell, G. M.; Salt, D. W. *Mol. Phys.* **1973**, *26* (4), 887−903.
(33) Jorge, M.; Seaton, N. A. *AICHE J.* **2003**, *49* (8), 2059−2070.
(34) Striolo, A.; Chialvo, A. A.; Cummings, P. T.; Gubbins, K. E. *Langmuir* **2003**, *19* (20), 8583−8591.
(35) Liu, J. C.; Monson, P. A. *Langmuir* **2005**, *21*, 10219−10225.
(36) Ghosh, S.; Ramanathan, K. V.; Sood, A. K. *Europhys. Lett.* **2004**, *65* (5), 678−684.
(37) Hanasaki, I.; Nakatani, A. *J. Chem. Phys.* **2006**, *124* (17) 174714.
(38) Kaneko, K.; Hanzawa, Y.; Iiyama, T.; Kanda, T.; Suzuki, T. *Adsorption: J. Internat. Adsorp. Soc.* **1999**, *5* (1), 7−13.
(39) Maniwa, Y.; Kataura, H.; Abe, M.; Suzuki, S.; Achiba, Y.; Kira, H.; Matsuda, K. *J. Phys. Soc. Jpn.* **2002**, *71* (12), 2863−2866.
(40) Mao, S. H.; Kleinhammes, A.; Wu, Y. *Chem. Phys. Lett.* **2006**, *421* (4−6), 513−517.
(41) Cossarutto, L.; Zimny, T.; Kaczmarczyk, J.; Siemieniewska, T.; Bimer, J.; Weber, J. V. *Carbon* **2001**, *39* (15), 2339−2346.
(42) Rudisill, E. N.; Hacskaylo, J. J.; Levan, M. D. *Ind. Eng. Chem. Res.* **1992**, *31* (4), 1122−1130.
(43) Salame, I.; Bandosz, T. J. *Langmuir* **1999**, *15* (2), 587−593.
(44) Alcaniz-Monge, J.; Linares-Solano, A.; Rand, B. *J. Phys. Chem. B* **2001**, *105* (33), 7998−8006.
(45) Easton, E. B.; Machin, W. D. *J. Colloid Interface Sci.* **2000**, *231* (1), 204−206.
(46) Sarkisov, L.; Monson, P. A. *Langmuir* **2000**, *16* (25), 9857−9860.
(47) Essam, J. W.; Fisher, M. E. *J. Chem. Phys.* **1963**, *38* (4), 802−812.
(48) Soper, A. K. *Chem. Phys.* **2000**, *258* (2−3), 121−137.
(49) Evans, R. *J. Phys.: Condens. Matter* **1990**, *2* (46), 8989−9007.
(50) Gelb, L. D.; Gubbins, K. E.; Radhakrishnan, R.; Sliwinska-Bartkowiak, M. *Rep. Prog. Phys.* **1999**, *62* (12), 1573−1659.
(51) Balbuena, P. B.; Gubbins, K. E. *Langmuir* **1993**, *9*, 1801−1814.
(52) Ball, P. C.; Evans, R. *Langmuir* **1989**, *5*, 714−723.
(53) Fowkes, F. M.; Harkins, W. D. *J. Am. Chem. Soc.* **1940**, *62*, 3377−3386.